CORE
Metadata, citation and similar papers at core.ac.uk
Provided by Nature Precedings

# Serine biosynthesis with one carbon catabolism represents a novel pathway for ATP generation in cells using alternative glycolysis with zero net ATP production

Alexei Vazquez[1,*] and Zoltán N. Oltvai[2]

[1]Department of Radiation Oncology, Bioinformatics & Surveillance, The Cancer Institute of New Jersey and UMDNJ-Robert-Wood Johnson Medical School, New Brunswick, NJ 08903, USA

[2]Department of Pathology, University of Pittsburgh School of Medicine, Pittsburgh, PA 15213, USA

* Corresponding author
Department of Radiation Oncology, Bioinformatics & Surveillance
The Cancer Institute of New Jersey
and UMDNJ-Robert-Wood Johnson Medical School
95 Little Albany Street, New Brunswick, NJ 08903, USA
Phone: 732-235-8918
Email: vazqueal@umdnj.edu

## Abstract

Recent experimental evidence indicates that some cancer cells have an alternative glycolysis pathway with net zero ATP production, implying that upregulation of glycolysis in these cells may not be related to the generation of ATP. Here we use a genome-scale model of human cell metabolism to investigate the potential metabolic alterations in cells using net zero ATP glycolysis. We uncover a novel pathway for ATP generation that involves reactions from the serine biosynthesis and one-carbon metabolism pathways. This pathway has a predicted two-fold higher flux rate in cells using net zero ATP glycolysis than those using standard glycolysis and generates twice as much ATP with significantly lower rate of lactate- but higher rate of alanine secretion. Thus, in cells using the standard- or the net zero ATP glycolysis pathways a significant portion of the glycolysis flux is always associated with ATP generation, and the ratio between the flux rates of the two pathways determines the rate of ATP generation and lactate and alanine secretion during glycolysis.

## Introduction

Oxidative phosphorylation (OxPhos) in the mitochondria is the major pathway for ATP generation in normal cells under normal oxygen conditions (normoxia), generating 32 mole of ATP per mole of glucose [1]. In contrast, under conditions of oxygen limitation (hypoxia), the mitochondrial activity is down-regulated and cells switch to glycolysis for ATP generation that yields only 2 mole of ATP per mole of glucose. Surprisingly, as first observed by Warburg [2], the metabolism of cancer cells is frequently characterized by a significant upregulation of glycolysis even under normoxic conditions, with both an increased glucose uptake and excretion of lactate (Warburg effect). More recently, it became evident that the Warburg effect is not unique to cancer cells alone. Indeed, both rapidly proliferating normal cells [3,4,5,6,7,8] and non-proliferating cells with high metabolic activity [9,10,11] display high levels of glycolysis with lactate excretion under normoxic conditions.

Despite the importance of OxPhos and aerobic glycolysis in ATP generation, more recent empirical evidence indicates that some cancer cells also utilize an alternative glycolysis pathway with net zero ATP generation [12]. This striking observation implies a physiological role for aerobic glycolysis other than ATP generation. One such role may be the capacity of glycolysis to fulfill the need of rapidly proliferating cells for precursor metabolites. However, it has been shown previously that the need for precursor metabolites in itself is not sufficient to explain the high glycolysis rates observed in proliferating cells [13,14]. Instead, molecular crowding and its resulting constraint on macromolecular concentrations is the key factor determining the Warburg effect [14,15]. The high density of macromolecules in the cell imposes limits on the total mitochondrial content per unit of cell volume and the total content of metabolic enzymes as well. In turn, the inherent limitation in mitochondrial density results in an upper bound on the maximum achievable OxPhos capacity. We have shown previously that this maximum is achieved at physiological conditions and that it results in a metabolic switch involving an upregulation of glycolysis and lactate excretion [14,15]. Yet, all these results were obtained making use of the standard glycolysis pathway, with a yield of 2 moles of ATP per mole of glucose.

Here we investigate the metabolic flux redistributions in proliferating cells that utilize the alternative glycolysis pathway with net zero ATP production [11]. To this end we improve on our previous flux balance model of human cell metabolism [14] by more precisely accounting for protein synthesis, including a self-consistent constraint that all ribosomal-, enzyme associated-, and non-metabolic proteins need to be accounted for by the rate of protein synthesis, which is proportional to the ribosomal density. We also make a more precise accounting of the molecular crowding constraint by considering mitochondria as a subcellular compartment independent from the cytosol. Using this model we uncover a novel pathway for ATP generation that involves reactions in the serine biosynthesis and one-carbon metabolism pathways. The flux rate of this pathway is predicted to be two-fold higher in cells with net zero ATP glycolysis relative to cells with the standard glycolysis. Furthermore, it accounts for most of the glycolysis rate in cells with net zero ATP glycolysis.

## Results

*Flux balance model of cell metabolism with molecular crowding constraint*

As starting point, we utilize a genome-scale metabolic reconstruction of a generic human cell [16] that includes most biochemical reactions catalyzed by enzymes encoded in the human genome. We add auxiliary reactions to represent nutrient uptake, excretion of metabolic byproducts, basal ATP demand needed for cell maintenance, basal rate of protein degradation, synthesis of cell biomass components (proteins, lipids, RNA and DNA) and cell proliferation (biomass components → cell) (Table S1, http://cinjweb.umdnj.edu/~vazqueal/fba_human.html). We assume that the cell is in a steady state where the production and consumption of every metabolite and macromolecules balances, known as the flux balance constraint [17]. We use $f_i$ to denote the steady state reaction rate (flux) of the $i$-th reaction in the metabolic network, where all reversible reactions are represented by a forward and backward rate, respectively. We use $\phi_c$ to denote the relative cell volume fraction occupied by the $c$-th cellular compartment, where a compartment represents the overall contribution of macromolecules of certain type (e.g., ribosomes) or of certain cell organelle (e.g., mitochondria). Specifically, here we consider proteins that do not form part of enzyme complexes or ribosomes (*P0*) and nutrients uptake systems (*NU*), all metabolic enzymes catalyzing reactions outside the mitochondria (*EnM*), all metabolic enzymes catalyzing reactions in the mitochondria (*EM*), ribosomes (*R*), and mitochondria (*M*). We assume the proliferation rate ($\mu$) and the total relative volume fraction occupied by macromolecules and organelles ($\phi_{max}$) are known and are given as input parameters of the model. Finally, we estimate the metabolic fluxes and compartment densities as the solution of the following optimization problem:

Find the $f_i$ and $\phi_c$ that minimize the sum of nutrient uptake rates

(1) $\Sigma_{i|NU} f_i$

subject to the metabolic constraints

(2) $\Sigma_i S_{mi} f_i = 0$ flux balance constraints

(3) $v_{i,min} \le f_i \le v_{i,max}$ minimum/maximum flux constraints

(4) $0 \le \phi_c \le \phi_{max}$ minimum/maximum volume fraction constraints

(5) $\Sigma_{i|EnM} a_i f_i \le \phi_{EnM}$ molecular crowding constraints

$\Sigma_{i|EM} a_i f_i \le \phi_M$

$a_R f_{protein\_synthesis} \le \phi_R$

$a_{M,ATP} f_{ATP\_synthase} \le \phi_M$

$\phi_{P0} + \phi_{EnM} + \phi_R + \phi_M \le \phi_{max}$

where $S_{mi}$ is the stoichiometric coefficient of metabolite $m$ in reaction $i$, $a_i = v_i/k_{eff,i}$ are the crowding coefficients of metabolic enzymes (enzyme molar volume / enzyme effective turnover)[18], $a_R = v_R/k_R$ is the ribosome crowding coefficient (ribosome molar volume / protein synthesis rate per ribosome), and $a_{M,ATP} = v_{s,M}/r_M$ the crowding coefficient of

mitochondria ATP generation (ATP synthesis rate per mitochondria mass / mitochondria specific volume) [14,15].

The estimation of all the model parameters is presented in the Methods section. Here we discuss some of them that deserve particular attention. The effective turnover numbers $k_{eff,i}$, quantify the reaction rate per enzyme molecule. For example, for an irreversible single substrate reaction satisfying Michaelis-Menten kinetics, $k_{eff}=kS/(K+S)$, where $k$ is the enzyme turnover number, $K$ the half-saturation concentration and $S$ the substrate concentration. The turnover numbers of some human enzymes are reported in the BRENDA database [19]. They have a typical value of 10 $sec^{-1}$ and a significant variation from 1 to 100 $sec^{-1}$ (Table S2, http://cinjweb.umdnj.edu/~vazqueal/fba_human.html). However, for most reactions we do not know the turnover number, the kinetic model, or the metabolite concentrations, impeding us to estimate $k_{eff}$. To cope with this indeterminacy we performed a sampling strategy, whereby the $k_{eff,i}$ were sampled from a reasonable range of values, and then focused on the predicted average behavior and 90% confidence intervals. The typical enzyme crowding coefficient is about $a_i$~0.00013 $(mM/min)^{-1}$, which is interpreted as follows: to maintain a reaction rate of 1 mM/min we need to allocate a relative cell volume of 0.00013 (0.013%) for the corresponding enzyme. The crowding coefficients are significantly larger for ribosomes and the mitochondria: $a_R$=3.6 $(mM/min)^{-1}$ and $a_{M,ATP}$=0.017 $(mM/min)^{-1}$, respectively.

The flux balance equation for proteins (equation (2) with *m=proteins*) is formulated more generally than before. Previous models have assumed a constant protein concentration and have not taken into account the self-consistent need to synthesize all the proteins in enzyme complexes and ribosomes [13,14]. In contrast, here we account for three major categories, proteins not associated with metabolism, proteins that are components of enzyme complexes, and ribosomal proteins, with their concentrations (moles/cell volume) denoted by $P_0$, $P_E$, and $P_R$, respectively. In proliferating cells, these concentrations will decrease at a rate $(\mu+k_D)(P_0+P_E+P_R)$, where $\mu$ denotes the proliferation rate and $k_D$ the basal rate of protein turnover. The total concentration of proteins in enzyme complexes can be estimated as $P_E=n_{PE}E=n_{PE}\Sigma_i f_i/k_{eff,i}$, where $n_{PE}$ is the average number of proteins in an enzyme complex (about 2.4) and $E$ is the total concentration of metabolic enzymes. Similarly, $P_R=n_{PR}\phi_R/\nu_R$, where $n_{PR}$ is the number of proteins in a ribosome (82 for the 80S ribosomes) and $\phi_R/\nu_R$ is the concentration of ribosomes. Putting all these elements together, the balance between protein turnover and synthesis implies $f_{Protein\_sysnthesis}=(\mu+k_D)[P_0+ n_{PE}\Sigma_i(f_i/k_{eff,i}) + (n_{PR}/\nu_R)\phi_R]$, where the term $(\mu+k_D)P_0$ is the only one considered in previous models [13,14,17]. In an effective manner, each metabolic reaction contributes to a component of protein synthesis, with a stoichiometric coefficient $(\mu+k_D)n_{PE}/k_{eff,i}$, quantifying the amount of protein necessary to keep the concentration of the corresponding enzyme constant. Similarly, a constant ribosome volume fraction also accounts for a component of protein synthesis, with a stoichiometric coefficient $(\mu+k_D)n_{PR}/\nu_R$, quantifying the amount of protein necessary to keep the ribosomes concentration constant. The rate of protein synthesis accounting for this effective protein dilution/degradation thus models the autocatalytic nature of cell

metabolism, whereby the macromolecular complexes catalyzing the metabolic reactions ultimately are themselves a product of metabolism.

To model the alternative glycolysis pathway we replaced the pyruvate kinase catalyzed reaction: Phosphoenolpyruvate + ADP + $H^+ \rightarrow$ Pyruvate + ATP, by the ATP independent reaction: Phosphoenolpyruvate + $H^+ \rightarrow$ Pyruvate + Phosphate. In the latter reaction phoshoglycerate mutase (PGM1) is the phosphate acceptor, which is then dephosphorylated by a yet unknown mechanism [12].

*Changes in the relative macromolecular densities with increased cell proliferation*

Figure 1 shows the predicted relative volume fraction occupied by non-mitochondrial enzymes ($\phi_{EnM}=\Sigma_{i|EnM}a_i f_i$), mitochondria ($\phi_M$), and ribosomes ($\phi_R$) as a function of the proliferation rate for cells growing in a medium containing glucose, glutamine, essential amino acids, and oxygen. The ribosomal density increases monotonically with increasing the proliferation rate in a nonlinear fashion, reaching a maximum of 10% of the cell volume at the highest proliferation rate of about 3/day (minimum doubling time of $\ln(2)/\mu_{max}$=5.5 hours) (Fig. 1, blue circles). At low proliferation rates, the mitochondrial density exhibits a wide range of values, overall occupying ~ 20% of the cell volume, and initially it increases with increasing the proliferation rate (Fig. 1, green triangles). However, beyond a proliferation rate of about 0.8/day (doubling time 21 hours), the mitochondrial density decreases with increasing the proliferation rate. This is in turn accompanied by a dramatic increase in the density of metabolic enzymes (Fig. 1, red squares). Our model thus predicts that when switching from low to high proliferation rates, the cell makes a transition from a mitochondria dominated molecular crowding regime to one dominated by enzymes + ribosomes (Fig. 1).

The impact of altering the different model parameters used on the behavior of the model can also be tested. Larger values of the mitochondrial crowding coefficient $a_M$, e.g., due to a decrease in mitochondrial efficiency for ATP generation, will cause a decrease of mitochondrial density at lower proliferation rates. Larger ribosome crowding coefficient $a_R$, e.g., due to a decrease in protein synthesis efficiency, will result in a faster increase of the ribosome density with increasing the proliferation rate, and a consequently faster decrease of the mitochondria density. Similarly, an increase in the average crowding coefficient of metabolic enzymes will cause a faster increase of the total enzyme concentration with increasing the proliferation, resulting in a faster decrease of the mitochondrial density as well. Cancer cells are characterized by partial alterations in all of these components, potentially resulting in a more dramatic effect than that depicted in Figure 1. In particular, mutations leading to damaged mitochondria will enhance the effect, as originally hypothesized by Warburg [2].

*Metabolic switch from low- to high proliferation rates*

The predicted transition in the macromolecular composition of the cell is accompanied by a global switch in the cell's metabolic state (Fig. 2). At the proliferation rate of about 0.8/day (doubling time 21 hours) the model predicts a substantial increase in

glucose uptake, sudden activation of glutamine uptake and α-ketoglutarate dehydrogenase activity, complete deactivation of pyruvate decarboxylase (PCm) and activation of the enzyme, pyruvate dehydrogenase (PDHm). The activity of pyruvate carboxylase in the low proliferation regime, where there is no glutamine uptake, is consistent with recent experimental data showing that pyruvate carboxylase is needed for growth without glutamine [20]. The activation of glutamine uptake at high proliferation rates is also in agreement with what have been observed experimentally [21]. We also observe activation of lactate excretion at high proliferation rates, the hallmark of the Warburg effect.

Several notable changes take place around the pyruvate branching point (Fig. 2). Most noticeably, the glycolysis pathway (Fig. 2) is truncated at 3-phosphoglycerate and the flux over the ATP-decoupled pyruvate kinase-catalyzed reaction is zero at all proliferation rates. We emphasize that we have not imposed a zero flux over this reaction, and the zero flux is a prediction of the model itself. Tryptophan is a source of pyruvate at low proliferation rates, with alanine as an intermediate metabolite (Fig. 2, tryptophan to pyruvate route, dashed lines). Alanine is converted to pyruvate by alanine transaminase, with concomitant transformation of α-ketoglutarate to glutamate. However, at high proliferation rates this reaction is reverted, producing alanine instead, which is then excreted. At high proliferation rates pyruvate is instead generated from glutamine (via malate). The cytosolic- (LDH-L) and mitochondrial L-lactate dehydrogenases (LDH-Lm) form a cycle between pyruvate and lactate. At low proliferation rates, LDH-Lm converts pyruvate to lactate and LDH-L converts lactate back to pyruvate, both reactions working at the same rate (Fig. 2, pyruvate-lactate loop, dashed lines). At high proliferation rates the cycle is reverted, LDH-L converting lactate to pyruvate and LDH-Lm pyruvate back to lactate (Fig. 2, pyruvate-lactate loop, solid lines). In the latter case the LDH-Lm catalyzed reaction has a higher rate, resulting in the net production of lactate, which is then excreted.

To provide evidence that the metabolic switch is a direct consequence of the molecular crowding constraint, we repeated the *in silico* analysis after removing this constraint (mathematically setting $\phi_{max}=\infty$ in equation (5)). Inspecting the changes in the reaction rates we observe that the metabolic switch it lost. The glucose uptake increases monotonically with increasing the proliferation rate (Fig. S1), but it does not manifest the same high rate of increase as with the molecular crowding constraint in place (Fig. 2). Furthermore, there is no lactate excretion at any proliferation rate (Fig. S1).

*Novel pathway for ATP generation*

When considering the molecular crowding constraint, our simulations show that at high proliferation rates most of the glycolysis rate is diverted towards the biosynthesis of serine (Fig. 2). However, this flux rate exceeds by more than 10 fold the serine requirements for protein synthesis (Fig. 2, serine to protein synthesis, top center panel). Therefore, we hypothesized that cells utilizing the net zero ATP glycolysis may overexpress some alternative pathway for ATP generation. To test this hypothesis we inspected the genome-scale reaction rate predictions, focusing on reactions producing ATP. Following this approach we identified the reactions with high rates of ATP

production in cells with a net zero ATP glycolysis at different proliferation rates. At low proliferation rates (0.03/day, doubling time 24 days) ATP synthase was the dominant reaction, supplying most of the ATP required for cell maintenance (Fig. 3a,b, left panels). On the other hand, at high proliferations rates (2.52/day, doubling time 6.6 hours) the formate-tetrahydrofolate ligase (FTHFL), working in the reverse direction to form ATP, is the dominant reaction (Fig. 3a, right panel). Formate-tetrahydrofolate ligase is also active in cells with the standard glycolysis (Fig. 3b, right panel). However, in the case of standard glycolysis phosphoglycerate kinase and pyruvate kinase are the dominant reactions at high proliferation rates (Fig. 3b, right panel).

By tracking back the flux from the formate-tetrahydrofolate ligase-catalyzed reaction to glycolysis we uncovered a novel pathway for ATP generation (Fig. 4). The pathway is composed of three main steps. First, *synthesis of L-serine* (ser-L) from the glycolysis intermediate metabolite 3-phosphoglycerate (3pg), using NAD and L-glutamate (glu-L) as cofactors (Fig. 4a), with the overall reaction

(6) $$\text{3-phosphoglycerate} + \text{L-glutamate} + NAD^+ + H_2O \rightarrow \text{L-gerine} + \alpha\text{-Ketoglutarate} + H^+ + NADH + \text{Phosphate}$$

Second, *the conversion of L-serine to glycine* with a concomitant one-carbon metabolism cycle, resulting in the net generation of 1 mole of ATP per mole of serine transformed, using NADP as a cofactor (Fig. 4b), with the overall reaction

(7) $$\text{L-Serine} + NADP + H_2O + ADP + \text{Phosphate} \rightarrow \text{Glycine} + NADPH + 2\,H^+ + ATP$$

Finally, *the conversion glycine to ammonium ($NH_4$)* in the mitochondria with a concomitant one-carbon metabolism cycle, using NAD and NADP as cofactors (Fig. 4c or d), with the overall reaction

(8) $$\text{Glycine} + NADP + NAD^+ + H_2O + ADP + \text{Phosphate} \rightarrow NH_4 + CO_2 + NADPH + NADH + 2\,H^+ + ATP$$

This pathway has a net yield of 2 mole of ATP per mole of 3-phosphoglycerate, therefore 4 mole of ATP per mole of glucose. Furthermore, when compared to the standard glycolysis, the net zero ATP glycolysis manifests a significant decrease in lactate excretion while increasing the alanine excretion (Fig. 2 a,b, right panel)

Although the reactions in the reaction cycle shown in Fig. 4b are all annotated as reversible in the human metabolic network reconstruction [16], the cycle may not work in the direction of ATP production due to thermodynamic constraints. Formate-tetrahydrofolate ligase (FTHFL) can efficiently catalyze the synthesis of ATP in the bacterium *Clostridium cylindrosporum* [22]. However, it remains to be elucidated whether this is also feasible in human cells, where the tri-functional enzyme $C_1$-tetrahydrofolate synthase is responsible for the methylene-tetrahydrofolate dehydrogenase (MTHFD), methenyl-tetrahydrofolate cyclohydrolase (MTHFC) and FTHFL activities. To address this issue, we have analyzed a kinetic model of the reaction cycle shown in Figure 4b, focusing on the cytosolic enzymes alone. The model is fully described in the Supporting Information and is based on a previous model of folate

metabolism [23]. We demonstrate that the kinetic model has a stable steady state in the direction of ATP production, indicating that the novel pathway is thermodynamically feasible.

## Discussion

The recent demonstration of an alternative glycolysis pathway with net zero ATP production in rapidly proliferating cells [12] challenged the general notion that the production of ATP is a major function of glycolysis. Instead, an alternative hypothesis suggests that the increased rate of glycolysis in rapidly proliferating cells is present to support the increased demand for precursor metabolites by anabolic processes involved in cell growth and proliferation [24]. However, based on a partial- or full genome-scale reconstruction of human cell metabolism [16,17] containing the standard glycolysis pathway we [14,15] and others [13] have shown that the anabolic requirements can be satisfied without the need for a dramatic upregulation of glycolysis and the excretion of lactate. We have recapitulated this result here, now using the alternative glycolysis pathway with net zero ATP production, providing *in silico* evidence that the demand for precursor metabolites can be satisfied without upregulation of the alternative glycolysis pathway (Fig. 2).

We have shown previously that molecular crowding is a major determinant of the metabolic changes observed in highly proliferating mammalian- [14,15] and prokaryotic cells [25,26] and in quiescent cells with high energy demands [14]. In essence, the high density of macromolecules in the intracellular millieu results in a 'competition' among mitochondria, ribosomes, metabolic enzymes and structural protein for the available intracellular space. At low metabolic rates this constraint is less pronounced, and therefore the density of the required organelles and macromolecules can increase to accommodate the increasing metabolic rate. However, much as just a finite number of people can be placed in a room, we can just fit a finite amount of mitochondria in the cell, resulting in an upper bound for OxPhos capacity. To satisfy its energetic needs beyond this maximum OxPhos capacity the cell need to switch to other pathways that are less costly in terms of the required relative fraction to allocate the corresponding enzymes, such as the classic glycolysis pathway. However, this hypothesis has been challenged by the observation that highly proliferating cells utilize an alternative glycolysis pathway with net zero ATP production [12]. To resolve this contradiction we have improved our genome-scale metabolic model of a human cell to be able to investigate the consequences of a net zero ATP production glycolysis.

The results of our *in silico* analyses yield several surprising observations. The glycolysis flux is upregulated in highly proliferating cells and it is routed from 3-phosphoglycerate toward serine biosynthesis. This prediction is supported by recent experimental observations in highly proliferating cells. Rapidly proliferating cells during embryonic development and cancer cells express a splice variant of pyruvate kinase (PKM2) that has low catalytic activity for the conversion of phosphoenol pyruvate to pyruvate, effectively reducing the rate over the last steps of glycolysis [12,27]. Serum-stimulation of Rat1A fibroblasts proliferation results in an increased $^{13}$C-labeled glycine derived from 3-phosphoglycerate, in a *myc* dependent manner [28]. In agreement with the

**Table I Overall reaction**

a) Standard glycolysis:

$$\text{Glucose} + 2\ \text{ADP} + 2\ \text{Phosphate} \rightarrow 2\ \text{Lactate} + 2\text{ATP} + 2\ H_2O + 2\ H^+$$

b) Novel ATP generating pathway:

$$\text{Glucose} + 2\ \text{L-glutamate} + 6\ NAD^+ + 4\ \text{NADP} + 6\ H_2O + 4\ \text{ADP} + 4\ \text{Phosphate} \rightarrow 2\ NH_4 + 2\ \alpha\text{-ketoglutarate} + 6\ \text{NADH} + 4\ \text{NADPH} + 4\ \text{ATP} + 14\ H^+ + 2\ CO_2$$

latter observation, gene expression microarray analyses have reported up-regulation of enzyme-encoding genes that catalyze one carbon metabolism in cancer cells [29,30]. These observations support the existence of an alternative glycolysis pathway with net zero ATP production and concomitant up-regulation of serine biosynthesis and one-carbon metabolism.

Our *in silico* approach allow us to investigate the fate of the high rate of the serine biosynthesis pathway. We discover that its final endpoint is a novel pathway for ATP generation, starting from the biosynthesis of serine and involving reactions in the one-carbon metabolism pathway (Fig. 4). The reaction responsible for the net ATP generation is catalyzed by formate-tetrahydrofolate ligase (EC 6.3.4.3), working in the ATP production direction. This pathway has a yield of 2 mole of ATP per mole of 3-phosphoglycerate, or 4 moles of ATP per mole of glucose. Taken together our *in silico* evidence indicates that, even in the context of an alternative glycolysis pathway with net zero ATP production, glycolysis is upregulated to satisfy the high energy demand of highly proliferating cells, during conditions where molecular crowding imposes a bound or a reduction in the mitochondrial density.

The novel pathway doubles the ATP yield from 2 to 4 mole of ATP per mole of glucose (Table I). The novel pathway requires, however, the balance of several co-factors and thus it is coupled to several other reactions. Yet, it remains to be elucidated what the potential evolutionary advantage of having two alternative glycolysis pathways is (i.e., the net zero ATP and the standard pathways) . As we show here, the novel pathway can generate two times more ATP, thus an energetic reason is probably likely. In contrast, the novel pathway involves 17 reactions, 7 more than the standard glycolysis, potentially contributing more to molecular crowding. Taken together with OxPhos, we obtain a hierarchy in terms of ATP yield: OxPhos >> net-zero-ATP-glycolysis > standard-glycolysis, and the same hierarchy in terms of molecular crowding. Therefore, these pathways provide the cell with different alternatives to cope with competing efficiency principles, ATP yield per mole of substrate or ATP yield per occupied volume fraction. Concomittantly, other factors, such as the cellular lactate and alanine production also has several potential advantages on the population level that may enhance the invasiveness of tumor cells. Also, tumor cells frequently encounter fluctuating hypoxia levels within growing tumors [31] requiring a capability to rapidly deploy alternative metabolic strategies [32]. In any event, our model identifies several metabolic changes that can be subject to further theoretical and experimental investigations.

## Material Methods

*Metabolic network reconstruction:* The reactions annotated in *H. sapiens* metabolic reconstruction 1 where downloaded from the BiGG database [16]. They are listed in Table S1, http://cinjweb.umdnj.edu/~vazqueal/fba_human.html, together with all auxiliary reactions.

*Crowding coefficients:* Dividing the mitochondrium specific volume (3.15 mL/g in mammalian liver [33] and 2.6 mL/g in muscle [34]) by the rate of ATP production per mitochondrial mass (0.1-1.0 mmol ATP/min/g [35,36,37]) we obtain $a_M$ values between 0.0026 to 0.032 min/mM. Except when specified, we use the median 0.017 min/mM. Dividing the ribosome molar volume ($v_R$ = 4,000 nm$^3$ × 6.02 10$^{23}$/mol=2.4 L/mmol) by the rate of protein synthesis per ribosome (0.67 proteins/min [38]) we obtain $a_R$=3.6 min/mM. The enzyme crowding coefficients were estimated as $a_i=v_E/k_i$. Multiplying the median molecular weight of human enzymes (98,750 g/mol, BRENDA [19], Table S2) by the enzymes specific volume (approximated by the specific volume of spherical proteins, 0.79 mL/g [39]) we obtain an estimated enzymes molar volume of $v_E$=0.078 L/mmol. The turnover numbers of human enzymes have significant variations from 1 to 100 sec$^{-1}$ (BRENDA, [19], Table S2). In the simulations log10($k_i$) was sampled uniformingly from the interval log10(1/sec) to log10(100/sec).

*Macromolecular composition:* Proteins were divided into three pools: ribosomal-, components of metabolic enzyme complexes-, and non-metabolic proteins. Each ribosome contributes to $n_{PR}$=82 proteins/ribosome (49 in the 60S and 33 in the 40S subunits [40]). The ribosomal protein concentration was computed as $P_R=n_{PR}\phi_R/v_R$. Each enzyme contributes with $n_{PE}$=2.4 proteins in average, estimated as median enzyme molecular weight (98,750 g/mol, reported above) divided by the median molecular weight of a human protein (40,835 g/mol). The median molecular weight of a human protein was estimated from the median protein length (355 amino acids [41]) and the typical amino acid composition [42]. The enzyme related protein concentration was computed as $P_E=\Sigma_i n_{PE} f_i/k_i$. The concentration of non-metabolic proteins was estimated as 85% (10% metabolic enzymes and 5% ribosomal protein [41]) of the reported total protein content per cell dry weight (0.018 mmol/g DW [42]), i.e. 0.015 mmol/g DW. The lipids, DNA and RNA composition were estimated by their relative abundance in a generic mammalian cell [42]. The abundance per cell dry weight were converted to concentrations after dividing by the typical cell specific volume 4.3 mL/g [43]. This resulted in a concentration of non-metabolic protein of $P_0$=3.59 mM. The maximum macromolecular density of human cells in the absence of osmotic stress is around $\phi_{max}$=40% [44].

*Maintenance parameters:* The ATP production rate necessary for cell maintenance is 1.55 mmol ATP/g DW/h [42]. The basal protein degradation rate was estimated as $k_D(P_0+P_E+P_R)$, where $k_D$=0.01/h [45].

*Simulations*: The optimization problem in equations (1)-(5) was solved in Matlab, using the linear programming function linprog. All reversible reactions were represented by an irreversible reaction on each direction with their own turnover number $k_i$. Most flux bounds were set to $v_{i,min}$=0 and $v_{i,max}$=∞, unless specified otherwise (Table S1).

*Kinetic model:* The kinetic model is described in the Supplementary Information.

## Figures

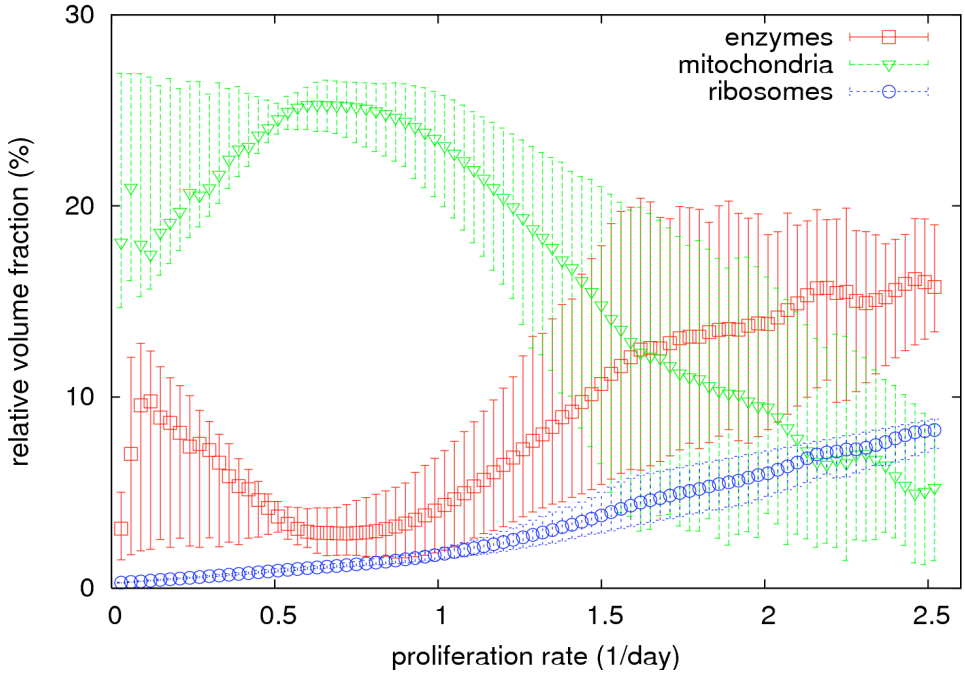


**Figure 1. Cell component densities at different proliferation rates:** Model predicted relative cell volume fraction occupied by metabolic enzymes (red squares), ribosomes (blue circles) and mitochondria (green triangles), respectively. The model-predicted median and 90% confidence intervals are shown.

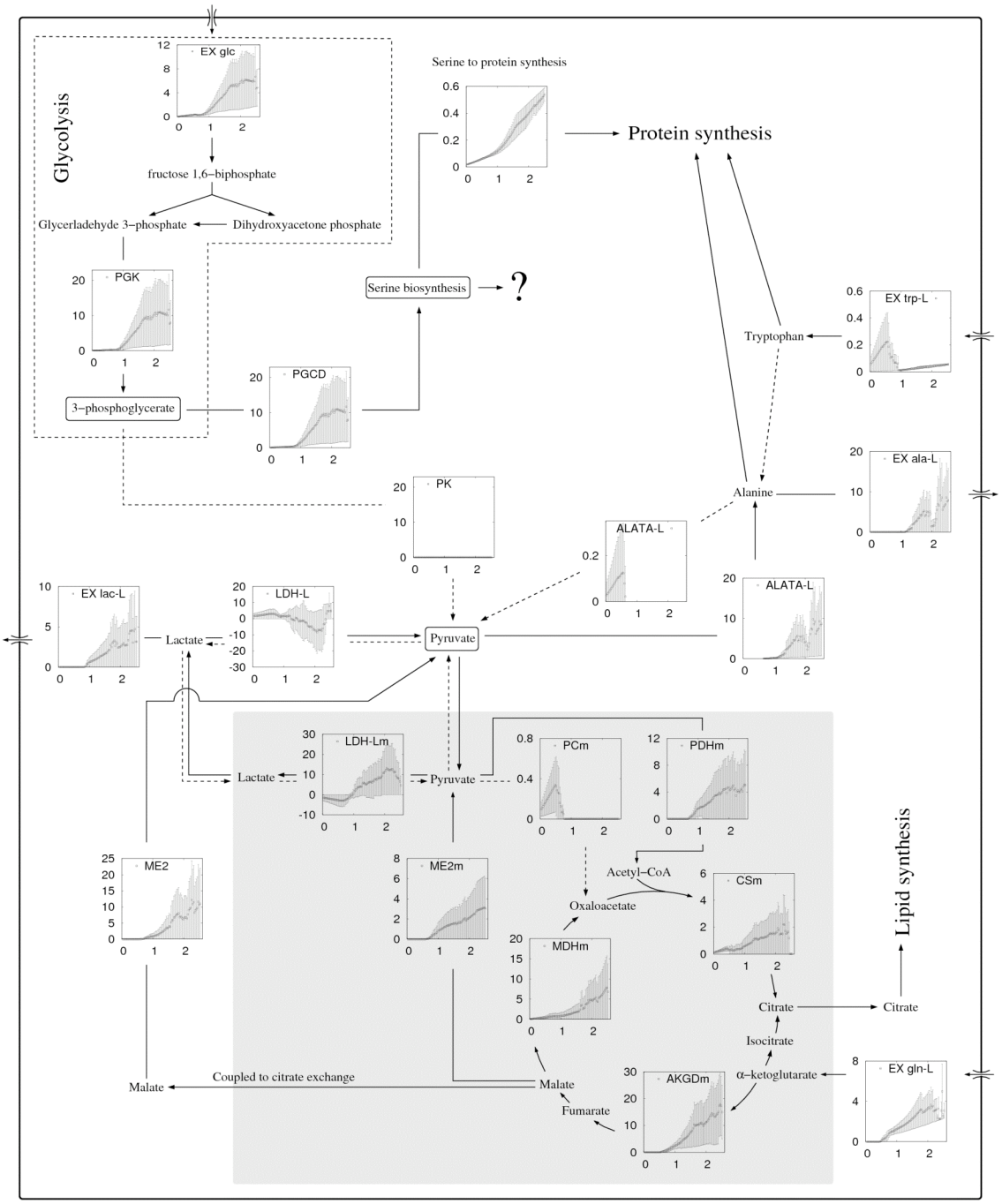


**Figure 2. Metabolic switch with increasing proliferation rate:** Selected metabolic reactions and pathways at different proliferation rates in cells utilizing the alternative glycolysis with net zero ATP production. The individual panels show the rate of the indicated reactions (vertical axis, mM/min) as a function of the proliferation rate (horizontal axis, 1/day). The gray shadow background contains reactions taking place in the mitochondria. Abbreviations: metabolite import/export (Ex metabolite: glc= glucose, gln=glutamine, Ala-L=alanine, trp-L=tryptophan, lac=lactate), phosphoglycerate kinase (PGK), pyruvate kinase (PK), phosphoglycerate dehydrogenase (PGCD), L-alanine transaminase (ALTA-L), L-lactate dehydroganse (LDH-L), malic enzyme (ME), malate dehydrogenase (MDH), pyruvate carboxylase (PC), pyruvate dehydrogenase (PDH), citrate synthase (CS), α-ketoglutarate dehydrogenase (AKGD).

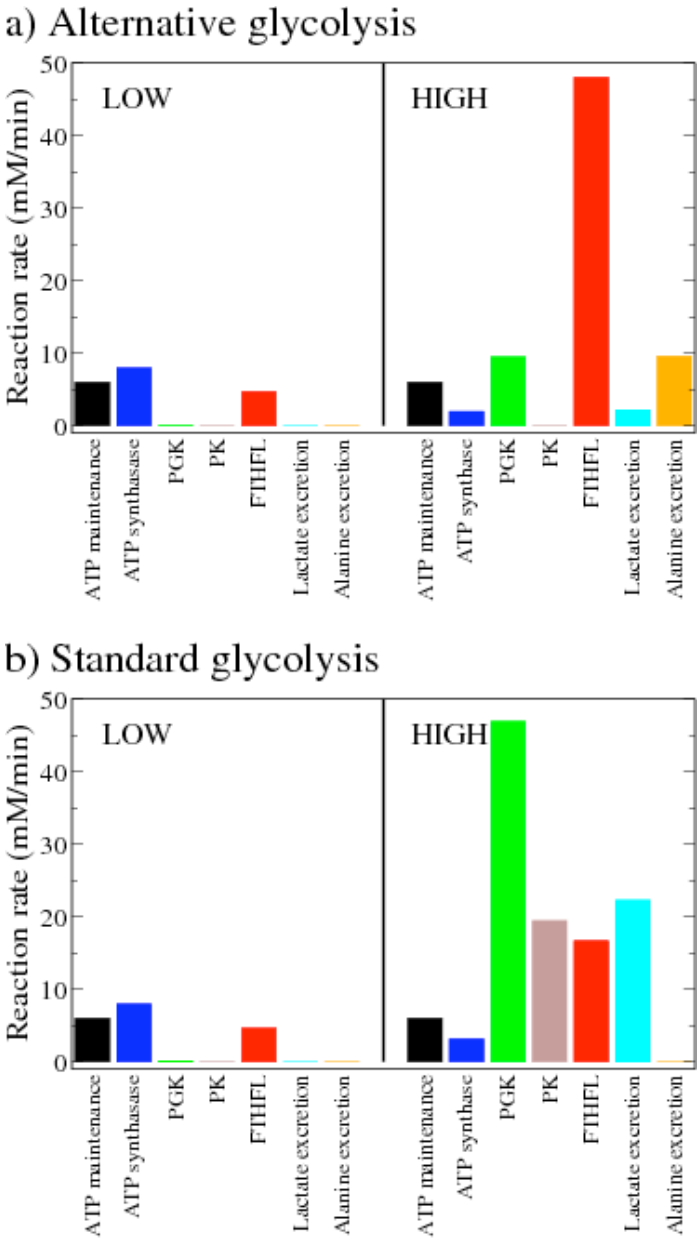


**Figure 3. Selected reactions contributing to ATP generation at different proliferation rates:** Contribution of ATP synthase, phosphoglycerate kinase (PGK), pyruvate kinase (PK) and formate-tetrahydrofolate ligase (FTHFL) to ATP generation in cells at low (0.03/day, left) and high (2.52/day, right) proliferation rates. The ATP consumed for cell maintenance (black) is shown as a reference. a) cells using the alternative glycolysis pathway with net zero ATP production. b) cells using the standard glycolysis.

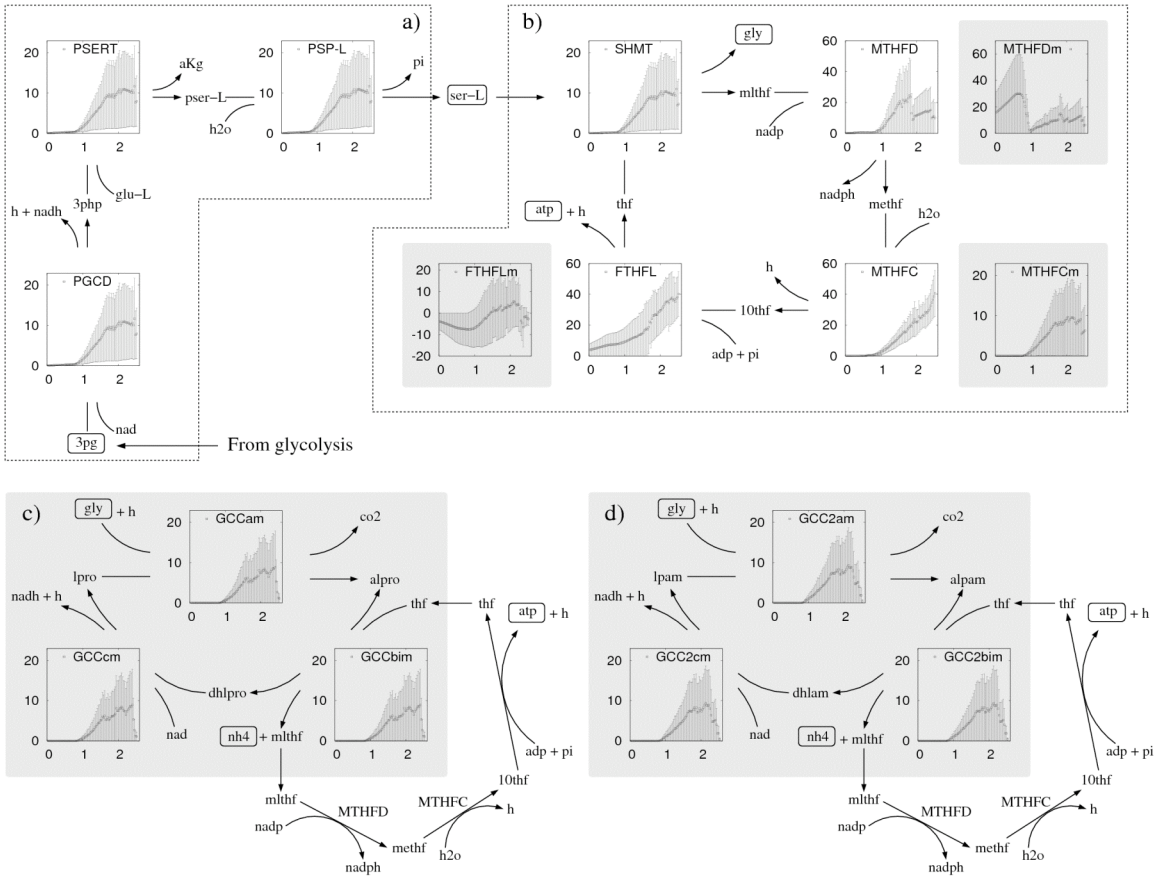


**Figure 4. Novel ATP producing pathway:** The fate of the high glycolysis flux in cells utilizing the alternative glycolysis [7]. The squared panels show the rate of the indicated reaction (vertical axis, in units of mM/min=mmol/min/L) as a function of the proliferation rate (horizontal axis, in units of 1/day). The gray shadow background contains reactions taking place in the mitochondria. Metabolite and enzyme abbreviations: 3-phosphoglycerate (3pg), phosphoglycerate dehydrogenase (PGCD), 3-phosphohydroxypyruvate (3php), L-glutamate (glu-L), phosphoserine transaminase (PSERT), α-ketoglutarate (aKg), L- phosphoserine (pser-L), phosphoserine phosphatase (PSP-L), L-serine (ser-L), tetrahydrofolate (thf), serine hydroxymethyltransferase (SHMT), glycine (gly), 5,10-methylene tetrahydrofolate (mlthf), methylenetetrahydrofolate dehydrogenase (MTHFD), 5,10-methenyl-tetrahydrofolate (methf), methenyltetrahydrofolate cyclohydrolase (MTHFC), 10-formyltetrahydrofolate (10thf), formate-tetrahydrofolate ligase (FTHFL), S-aminomethyldihydrolipoylprotein (alpro), dyhydrolipolprotein (dhlpro), lipoylprotein (lpro), S-aminomethyldihydrolipoamide (alpam), dihydrolipoamide (dhlam), and lipoamide (lpam). glycine-cleavage complex with lipoylprotein (GCCam, GCCbim and GCCcm) and glycine-cleavage complex with lipoamide (GCC2am, GCC2bim and GCC2cm).

## References


1. Voet D, Voet JG, Pratt CW (2006) Fundamentals of biochemistry: life at the molecular level. New York: Wiley. 1 v. (various pagings) p.
2. Warburg O (1956) On the origin of cancer cells. Science 123: 309-314.
3. Wang T, Marquardt C, Foker J (1976) Aerobic glycolysis during lymphocyte proliferation. Nature 261: 702-705.
4. Hume DA, Radik JL, Ferber E, Weidemann MJ (1978) Aerobic glycolysis and lymphocyte transformation. Biochem J 174: 703-709.
5. Parra-Bonilla G, Alvarez DF, Al-Mehdi AB, Alexeyev M, Stevens T (2010) Critical role for lactate dehydrogenase A in aerobic glycolysis that sustains pulmonary microvascular endothelial cell proliferation. Am J Physiol Lung Cell Mol Physiol 299: L513-522.
6. Williams R, Philpott MP, Kealey T (1993) Metabolism of freshly isolated human hair follicles capable of hair elongation: a glutaminolytic, aerobic glycolytic tissue. J Invest Dermatol 100: 834-840.
7. Munyon WH, Merchant DJ (1959) The relation between glucose utilization, lactic acid production and utilization and the growth cycle of L strain fibroblasts. Exp Cell Res 17: 490-498.
8. Trabold O, Wagner S, Wicke C, Scheuenstuhl H, Hussain MZ, et al. (2003) Lactate and oxygen constitute a fundamental regulatory mechanism in wound healing. Wound Repair Regen 11: 504-509.
9. Farrell PA, Wilmore JH, Coyle EF, Billing JE, Costill DL (1979) Plasma lactate accumulation and distance running performance. Med Sci Sports 11: 338-344.
10. Joyner MJ, Coyle EF (2008) Endurance exercise performance: the physiology of champions. J Physiol 586: 35-44.
11. Lemons JM, Feng XJ, Bennett BD, Legesse-Miller A, Johnson EL, et al. (2010) Quiescent fibroblasts exhibit high metabolic activity. PLoS Biol 8: e1000514.
12. Vander Heiden MG, Locasale JW, Swanson KD, Sharfi H, Heffron GJ, et al. (2010) Evidence for an alternative glycolytic pathway in rapidly proliferating cells. Science 329: 1492-1499.
13. Shlomi T, Benyamini T, Gottlieb E, Sharan R, Ruppin E (2011) Genome-scale metabolic modeling elucidates the role of proliferative adaptation in causing the warburg effect. PLoS Comput Biol 7: e1002018.
14. Vazquez A, Oltvai ZN (2011) Molecular crowding defines a common origin for the warburg effect in proliferating cells and the lactate threshold in muscle physiology. Plos One 6: e19538.
15. Vazquez A, Liu J, Zhou Y, Oltvai ZN (2010) Catabolic efficiency of aerobic glycolysis: the Warburg effect revisited. BMC Syst Biol 4: 58.
16. Schellenberger J, Park JO, Conrad TM, Palsson BO (2010) BiGG: a Biochemical Genetic and Genomic knowledgebase of large scale metabolic reconstructions. BMC Bioinformatics 11: 213.
17. Mo ML, Jamshidi N, Palsson BO (2007) A genome-scale, constraint-based approach to systems biology of human metabolism. Mol Biosyst 3: 598-603.
18. Vazquez A, de Menezes MA, Barabasi AL, Oltvai ZN (2008) Impact of limited solvent capacity on metabolic rate, enzyme activities, and metabolite concentrations of S. cerevisiae glycolysis. PLoS Comput Biol 4: e1000195.

19. Schomburg I, Chang A, Schomburg D (2002) BRENDA, enzyme data and metabolic information. Nucleic Acids Res 30: 47-49.
20. Cheng T, Sudderth J, Yang C, Mullen AR, Jin ES, et al. (2011) Pyruvate carboxylase is required for glutamine-independent growth of tumor cells. Proc Natl Acad Sci U S A 108: 8674-8679.
21. Wise DR, DeBerardinis RJ, Mancuso A, Sayed N, Zhang XY, et al. (2008) Myc regulates a transcriptional program that stimulates mitochondrial glutaminolysis and leads to glutamine addiction. Proc Natl Acad Sci U S A 105: 18782-18787.
22. Curthoys NP, Rabinowitz JC (1972) Formyltetrahydrofolate synthetase. Binding of folate substrates and kinetics of the reverse reaction. J Biol Chem 247: 1965-1971.
23. Nijhout HF, Reed MC, Budu P, Ulrich CM (2004) A mathematical model of the folate cycle: new insights into folate homeostasis. J Biol Chem 279: 55008-55016.
24. Vander Heiden MG, Cantley LC, Thompson CB (2009) Understanding the Warburg effect: the metabolic requirements of cell proliferation. Science 324: 1029-1033.
25. Beg QK, Vazquez A, Ernst J, de Menezes MA, Bar-Joseph Z, et al. (2007) Intracellular crowding defines the mode and sequence of substrate uptake by Escherichia coli and constrains its metabolic activity. Proc Natl Acad Sci U S A 104: 12663-12668.
26. Vazquez A, Beg QK, Demenezes MA, Ernst J, Bar-Joseph Z, et al. (2008) Impact of the solvent capacity constraint on E. coli metabolism. BMC Syst Biol 2: 7.
27. Christofk HR, Vander Heiden MG, Harris MH, Ramanathan A, Gerszten RE, et al. (2008) The M2 splice isoform of pyruvate kinase is important for cancer metabolism and tumour growth. Nature 452: 230-233.
28. Morrish F, Isern N, Sadilek M, Jeffrey M, Hockenbery DM (2009) c-Myc activates multiple metabolic networks to generate substrates for cell-cycle entry. Oncogene 28: 2485-2491.
29. Nikiforov MA, Chandriani S, O'Connell B, Petrenko O, Kotenko I, et al. (2002) A functional screen for Myc-responsive genes reveals serine hydroxymethyltransferase, a major source of the one-carbon unit for cell metabolism. Molecular and Cellular Biology 22: 5793-5800.
30. Palaskas NJ, Larson SM, Schultz N, Komisopoulou E, Wong J, et al. (2011) 18F-fluorodeoxy-glucose positron emission tomography (18FDG-PET) marks MYC-overexpressing human basal-like breast cancers. Cancer Res (In press).
31. Cardenas-Navia LI, Mace D, Richardson RA, Wilson DF, Shan S, et al. (2008) The pervasive presence of fluctuating oxygenation in tumors. Cancer Res 68: 5812-5819.
32. Semenza GL (2008) Tumor metabolism: cancer cells give and take lactate. J Clin Invest 118: 3835-3837.
33. Glas U, Bahr GF (1966) Quantitative study of mitochondria in rat liver. Dry mass, wet mass, volume, and concentration of solids. J Cell Biol 29: 507-523.
34. Schwerzmann K, Hoppeler H, Kayar SR, Weibel ER (1989) Oxidative capacity of muscle and mitochondria: correlation of physiological, biochemical, and morphometric characteristics. Proc Natl Acad Sci U S A 86: 1583-1587.

35. Wibom R, Hultman E, Johansson M, Matherei K, Constantin-Teodosiu D, et al. (1992) Adaptation of mitochondrial ATP production in human skeletal muscle to endurance training and detraining. J Appl Physiol 73: 2004-2010.
36. Short KR, Nygren J, Barazzoni R, Levine J, Nair KS (2001) T(3) increases mitochondrial ATP production in oxidative muscle despite increased expression of UCP2 and -3. Am J Physiol Endocrinol Metab 280: E761-769.
37. Hou XY, Green S, Askew CD, Barker G, Green A, et al. (2002) Skeletal muscle mitochondrial ATP production rate and walking performance in peripheral arterial disease. Clin Physiol Funct Imaging 22: 226-232.
38. Princiotta MF, Finzi D, Qian SB, Gibbs J, Schuchmann S, et al. (2003) Quantitating protein synthesis, degradation, and endogenous antigen processing. Immunity 18: 343-354.
39. Lee B (1983) Calculation of volume fluctuation for globular protein models. Proc Natl Acad Sci U S A 80: 622-626.
40. Alberts B (2008) Molecular biology of the cell. New York, N.Y.,: Garland Science. xxxiii, 1601p. p.
41. Brocchieri L, Karlin S (2005) Protein length in eukaryotic and prokaryotic proteomes. Nucleic Acids Res 33: 3390-3400.
42. Sheikh K, Forster J, Nielsen LK (2005) Modeling hybridoma cell metabolism using a generic genome-scale metabolic model of Mus musculus. Biotechnol Prog 21: 112-121.
43. Frame KK, Hu WS (1990) Cell volume measurement as an estimation of mammalian cell biomass. Biotechnol Bioeng 36: 191-197.
44. Zhou EH, Trepat X, Park CY, Lenormand G, Oliver MN, et al. (2009) Universal behavior of the osmotically compressed cell and its analogy to the colloidal glass transition. Proc Natl Acad Sci U S A 106: 10632-10637.
45. Savinell JM, Palsson BO (1992) Network analysis of intermediary metabolism using linear optimization. I. Development of mathematical formalism. J Theor Biol 154: 421-454.

**Figure S1**

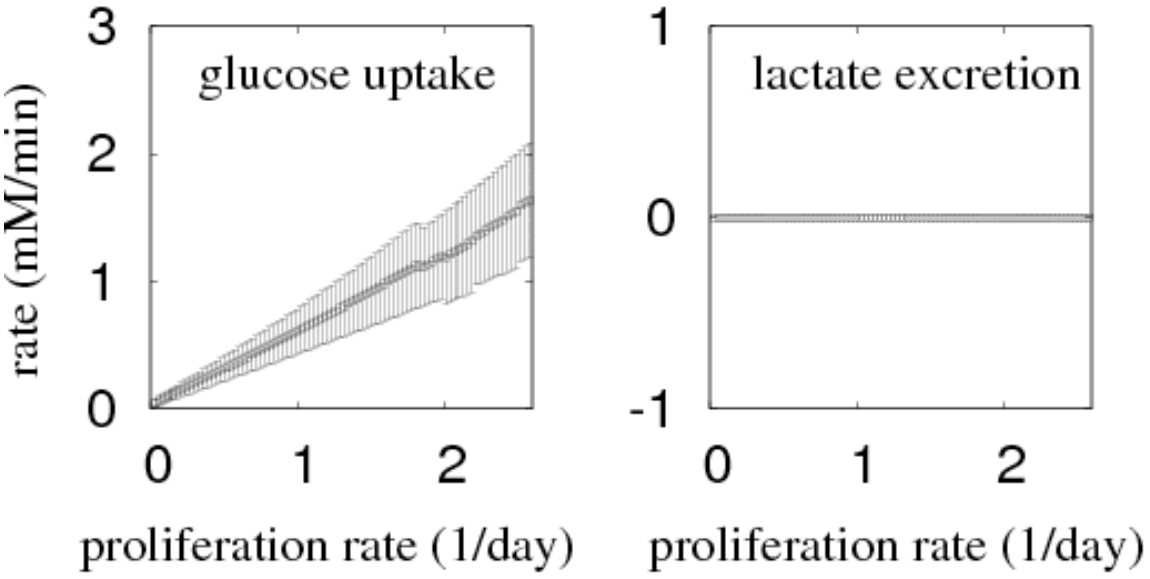
glucose uptake
lactate excretion
rate (mM/min)
3
2
1
0
1
0
-1
0
1
2
0
1
2
proliferation rate (1/day)
proliferation rate (1/day)

# Supplementary Material

### Kinetic model of the Fig. 3b module

Although the reactions in the reaction cycle shown in Figure 4b of the main text are all annotated as reversible, the cycle may not work in the direction of ATP production due to thermodynamic constraints. To address this issue, we analyze a kinetic model of the reaction cycle shown in Figure 4b, focusing on the cytosolic enzymes alone. The model is fully described in the Supporting Information and was based on a previous model of folate metabolism [1]. The four reactions in Fig. 3b are modeled as revesersible random multimolecular reactions

$$\begin{aligned} f_{SHMT} &= \left\{ k_{SHMT,f} \frac{[thf]}{K_{SHMT,thf} + [thf]} \frac{[ser-L]}{K_{SHMT,ser-L} + [ser-L]} \right. \\ &- \left. k_{SHMT,r} \frac{[mlthf]}{K_{SHMT,mlthf} + [mlthf]} \frac{[gly]}{K_{SHMT,gly} + [gly]} \right\} E_{SHMT} \end{aligned} \tag{1}$$

$$\begin{aligned} f_{MTHFD} &= \left\{ k_{MTHFD,f} \frac{[mlthf]}{K_{MTHFD,mlthf} + [mlthf]} \frac{[nadp]}{K_{MTHFD,nadp} + [nadp]} \right. \\ &- \left. k_{MTHFD,r} \frac{[methf]}{K_{MTHFD,methf} + [methf]} \frac{[nadph]}{K_{MTHFD,nadph} + [nadph]} \right\} E_{MTHFD1} \end{aligned} \tag{2}$$

$$\begin{aligned} f_{MTHFC} &= \left\{ k_{MTHFC,f} \frac{[methf]}{K_{MTHFC,methf} + [methf]} \right. \\ &- \left. k_{MTHFC,r} \frac{[10fthf]}{K_{MTHFC,10fthf} + [10fthf]} \right\} E_{MTHFD1} \end{aligned} \tag{3}$$

$$\begin{aligned} f_{FTHFL} &= \left\{ k_{FTHFL,f} \frac{[10fthf]}{K_{FTHFL,10fthf} + [10fthf]} \frac{[adp]}{K_{FTHFL,adp} + [adp]} \frac{[pi]}{K_{FTHFL,pi} + [pi]} \right. \\ &- \left. k_{FTHFL,r} \frac{[thf]}{K_{FTHFL,thf} + [thf]} \frac{[atp]}{K_{FTHFL,atp} + [atp]} \frac{[for]}{K_{FTHFL,for} + [for]} \right\} E_{MTHFD1} \end{aligned} \tag{4}$$

where $f_{reaction}$ denotes the net reaction rate, $k_{reaction,f}$ and $k_{reaction,r}$ forward and backward turnover numbers, $K_{reaction,metabolite}$ the half-saturation constant, $[metabolite]$ the corresponding metabolite concentration, and $E_{enzyme}$ the concentration of the corresponding enzyme. Here the following abbreviations have been used: tetrahydrofolate (thf), 5,10-methylene hydrofolate (mlthf), 5,10-methenyltetrahydrofolate (methf), 10-formyltetrahydrofolate (10fthf), L-serine (ser-L), glycine (gly), formate (for), serine hydroxymethyltransferase (SHMT), methylenetetrahydrofolate dehydrogenase (MTHFD), methenyltetrahydrofolate cyclohydrolase (MTHFC), and 5-formethyltetrahydrofolate cycloligase (FTHFL). We note in human cells the MTHFD, MTHFC and FTHFL activities are carried on by a tri-functional enzyme encoded by the MTHD1. The kinetic parameter values are reported in Table S3. These parameters where obtained from [1] or through references cited in the BRENDA database [2]. In humans the cytosolic enzyme activities of MTHFD, MTHFC and FTHFL are carried by the tri-functional enzyme C1-tetrahydrofolate synthase [3], encoded by the SMTHFD1 gene. Therefore, the reaction cycle shown in Figure 4b is regulated by the activity of two enzymes, serine hydroxymethyltransferase (SHMT) and C1-tetrahydrofolate synthase (SMTHFD1). The total concentration of these two enzymes ESHMT+SMTHFD1 determines how fast the system evolves to a steady state and the absolute rate at steady state, but it has no impact on the metabolite concentrations at steady state. Taking this fact into consideration we focus on the system behavior as a function of the relative concentration of one of the enzymes, SHMT for example $E_{SMTHFD1}/(E_{SHMT} + E_{SMTHFD1})$.

We focus our analysis on the concentrations of the intermediate metabolites thf, mlthf, methf and 10fthf, assuming the concentration of ser-L, glyc, formate, co-factors and enzymes constant, and given as input parameters of the model (Table S3, below). The concentration of intermediate metabolites evolve in time following the first order differential equations

$$\frac{d[thf]}{dt} = f_{FTHFL}([thf], [10fthf]) - f_{SHMT}([mlthf], [thf]) \tag{5}$$

$$\frac{d[mlthf]}{dt} = f_{SHMT}([mlthf],[thf]) - f_{MTHFC}([mlthf],[methf]) \tag{6}$$

$$\frac{d[methf]}{dt} = f_{MTHFC}([mlthf],[methf]) - f_{MTHFD}([methf],[10fthf]) \tag{7}$$

$$\frac{d[thf]}{dt} = f_{MTHFD}([methf],[10fthf]) - f_{FTHFL}([10fthf],[thf]) \tag{8}$$

Our aim is to determine whether this dynamical system has a steady state with in the direction of producing ATP. To this end we numecarically determined the fixed point of (5)-(8) that resulted in the highest steady state flux with ATP production. This was accomplished solving the optimization problem:

$$\text{Maximize } f_{FTHFL}([mlthf],[thf]) \tag{9}$$

subject to the fixed point constraints

$$\frac{d[thf]}{dt} = \frac{d[mlthf]}{dt} = \frac{d[methf]}{dt} = \frac{d[thf]}{dt} = 0 \tag{10}$$

and the metabolite concentration bounds

$$0 \leq [thf] \leq [thf]_{max}$$

$$0 \leq [mlthf] \leq [mlthf]_{max}$$

$$0 \leq [methf] \leq [methf]_{max}$$

$$0 \leq [10fthf] \leq [10fthf]_{max} \tag{11}$$

The problem was solved in Matlab using the function `fmicon`, with all upper bounds equal to 1 mM.

For all $0 < E_{SMTHFD1}/(E_{SHMT} + E_{SMTHFD1}) < 1$ the steady state with maximum rate is characterized by a positive rate of ATP production (Fig. S2, green cicrles), indicating that the reaction cycle shown in Figure 4b is thermodynamically feasible in the direction of ATP production. The maximum rate is achieved at a relative concentration $E_{SMTHFD1}/(E_{SHMT} + E_{SMTHFD1})$ around 0.05. Hence, the cycle achieves higher rates when the relative concentration of SMTHFD1 is much higher than that of SHMT. We also note the maximum rate calculated from the specified kinetic parameters is much higher than the median obtained from simulations applying a two-fold change in the model kinetic parameters (Fig. S2, red squares). This could indicate that the kinetic parameters in this pathway have been selected for maximum ATP production. However, since the curve for the observed kinetic parameters is still within the 90% confidence intervals (Fig. S2, red errorbars) we cannot exclude this is just coincidence.

| Parameter | Value | Source |
|---|---|---|
| SHMT | | |
| $k_{SHMT,f}$ | 9.58 | [3] |
| $k_{SHMT,r}$ | 0.60 | Estimated as $k_{SHMT,f}V_{max,r}/V_{max,f}$ |
| $V_{max,f}$ | 40,000 | [1] |
| $V_{max,r}$ | 25,000 | [1] |
| $K_{SHMT,thf}$ | 0.05 | [1] |
| $K_{SHMT,ser-L}$ | 0.6 | [1] |
| $K_{SHMT,mlthf}$ | 3.2 | [1] |
| $K_{SHMT,gly}$ | 10 | [1] |
| MTHFD | | |
| $k_{MTHFD,f}$ | 10 | [4] |
| $k_{MTHFD,r}$ | | $k_{MTHFD,f}V_{max,r}/V_{max,f}$ |
| $V_{max,f}$ | 200,000 | [1] |
| $V_{max,r}$ | 594,000 | [1] |
| $K_{MTHFD,mlthf}$ | 0.002 | [1] |
| $K_{MTHFD,nadp}$ | 0.022 | [4] |
| $K_{MTHFD,methf}$ | 0.01 | [1] |
| $K_{MTHFD,nadph}$ | 0.022 | Estimated as $K_{MTHFD,nadph}$ |
| $[nadp]$ | 0.02 | [5] |
| $[nadph]$ | 0.01 | [5] |
| MTHFC | | |
| $k_{MTHFC,f}$ | 134 | [6] |
| $k_{MTHFC,r}$ | 3.35 | Estimated as $k_{MTHFC,f}V_{max,r}/V_{max,f}$ |
| $V_{max,f}$ | 800,000 | [1] |
| $V_{max,r}$ | 20,000 | [1] |
| $K_{MTHFC,methf}$ | 250 | [1] |
| $K_{MTHFC,10fthf}$ | 100 | [1] |
| FTHFL | | |
| $k_{FTHFL,f}$ | 0.23 | Estimated from (4) at equilibrium ($f_{FTHFL} = 0$) |
| $[10fthf]_{eq}$ | 4 | *Clostridium cylindrosporum* [7] |
| $[adp]_{eq}$ | 4 | *Clostridium cylindrosporum* [7] |
| $[pi]_{eq}$ | 4 | *Clostridium cylindrosporum* [7] |
| $[thf]_{eq}$ | 0.9 | *Clostridium cylindrosporum* [7] |
| $[atp]_{eq}$ | 0.8 | *Clostridium cylindrosporum* [7] |
| $[for]_{eq}$ | 2.3 | *Clostridium cylindrosporum* [7] |
| $k_{FTHFL,r}$ | 0.0364 | [8] |
| $K_{FTHFL,10fthf}$ | 10 | *Clostridium cylindrosporum* [9] |
| $K_{FTHFL,adp}$ | 0.0364 | [8] |
| $K_{FTHFL,pi}$ | 4 | [8] |
| $K_{FTHFL,thf}$ | 0.364 | [8] |
| $K_{FTHFL,atp}$ | 0.0302 | [8] |
| $K_{FTHFL,for}$ | 0.0367 | [8] |
| $[adp]$ | 0.011 | [10] |
| $[pi]$ | 6 | [10] |
| $[atp]$ | 5 | [10] |
| $[for]$ | 0.9 | [1] |

**Table S3: Model parameters.** All half-saturation constants $K_{reaction,metabolite}$ and metabolite concentrations $[metabolite]$ are expressed in mM and all turnover numbers $k_{reaction,direction}$ in 1/sec.

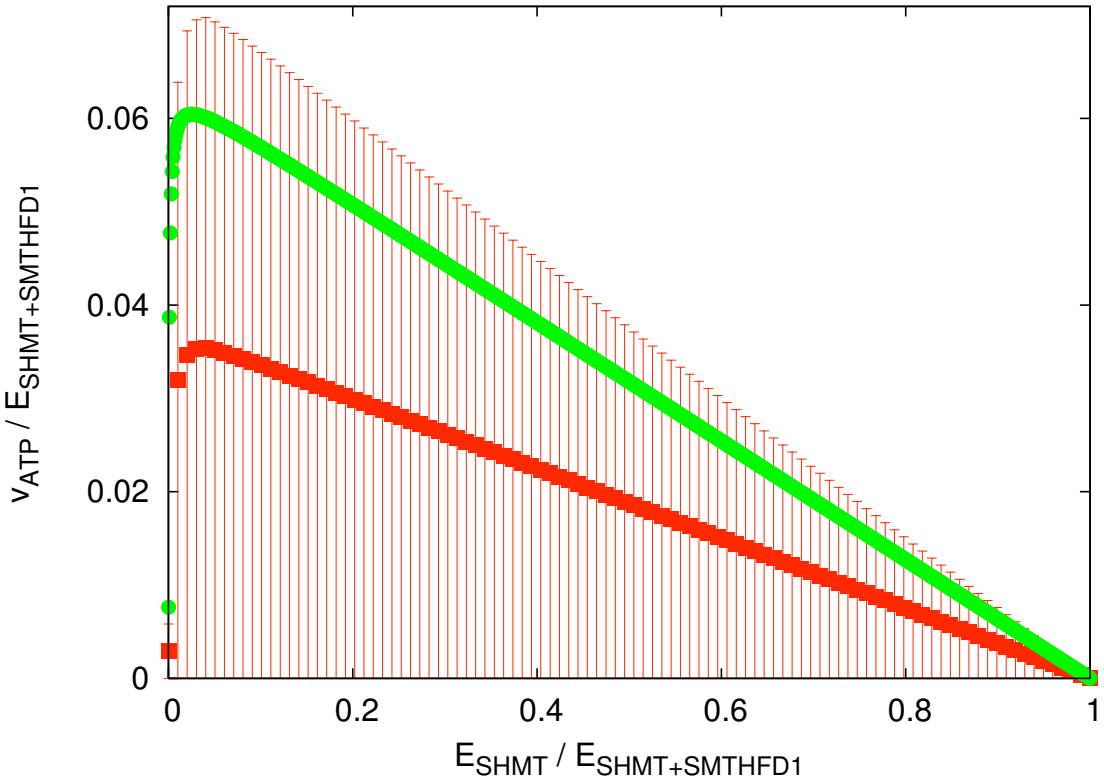


**Figure S2: Kinetic properties of the reaction cycle shown in Figure 4b.** Maximum ATP production rate of cycle in Figure 4b as a function of $E_{SMTHFD1}/(E_{SHMT} + E_{SMTHFD1})$. The green squares were obtained using the kinetic parameters reported in Table S3. The red squares and errorbars represent the median and 90% confidence interval over 100 simulated kinetic parameters, where the logarithm of each kinetic parameter was sampled uniformingly from a value two fold lower to a value two fold higher than the value in Table S3.


[1] Nijhout HF, Reed MC, Budu P, Ulrich CM (2004) A mathematical model of the folate cycle: new insights into folate homeostasis. J Biol Chem 279:55008-16.

[2] Scheer M, Grote A, Chang A, Schomburg I, Munaretto C, Rother M, Söhngen C, Stelzer M, Thiele J, Schomburg D (2011) BRENDA, the enzyme information system in 2011. Nucleic Acids Res 39:D670-6.

[3] Kruschwitz H, Ren S, Di Salvo M, Schirch V (1995) Expression, purification, and characterization of human cytosolic serine hydroxymethyltransferase. Protein Expr Purif 6:411-6.

[4] Pawelek PD, MacKenzie RE (1998) Methenyltetrahydrofolate cyclohydrolase is rate limiting for the enzymatic conversion of 10-formyltetrahydrofolate to 5,10-methylenetetrahydrofolate in bifunctional dehydrogenase-cyclohydrolase enzymes. Biochemistry 37:1109-15.

[5] Pinkas-Sarafova A, Markova NG, Simon M (2005) Dynamic changes in nicotinamide pyridine dinucleotide content in normal human epidermal keratinocytes and their effect on retinoic acid biosynthesis. Biochem Biophys Res Commun 336:554-64.

[6] Pawelek PD, Allaire M, Cygler M, MacKenzie RE (2000) Channeling efficiency in the bifunctional methylenetetrahydrofolate dehydrogenase/cyclohydrolase domain: the effects of site-directed mutagenesis of NADP binding residues. Biochim Biophys Acta 1479:59-68.

[7] Himes RH, Rabinowitz JC (1962) Formyltetrahydrofolate synthetase. II. Characteristics of the enzyme and the enzymic reaction. J Biol Chem 237:2903-14.

[8] Christensen KE, Rohlicek CV, Andelfinger GU, Michaud J, Bigras JL, Richter A, Mackenzie RE, Rozen R (2009) The MTHFD1 p.Arg653Gln variant alters enzyme function and increases risk for congenital heart defects. Hum Mutat :212-20.

[9] Buttlaire DH (1980) Purification and properties of formyltetrahydrofolate synthetase. Methods Enzymol 66:585-99.

[10] Kushmerick MJ, Moerland TS, Wiseman RW (1992) Mammalian skeletal muscle fibers distinguished by contents of phosphocreatine, ATP, and Pi. Proc Natl Acad Sci USA 897521-5.